PLEASE CITE THIS ARTICLE AS DOI: 10.1063/5.0205013

6/2/2024 RSI24-AR-00370

A platform for planar dynamic compression of crystalline hydrogen toward the terapascal regime

A. K. Schwemmlein,*^{1,2} G. W. Collins,^{1,2} A. J. LaPierre,^{2,3} Z. K. Sprowal,^{1,2} D. N. Polsin,^{1,2} R. Jeanloz,⁴ P. M. Celliers⁵, J. H. Eggert⁵ and J. R. Rygg^{1,2}

¹Department of Mechanical Engineering, University of Rochester, Rochester, New York, 14620, USA

We describe a method for laser-driven planar compression of crystalline hydrogen that starts with a sample of solid para-hydrogen (even-valued rotational quantum number j) having an entropy of 0.06 k_B /molecule at 10 K and 2 atm, with Boltzmann constant k_B . Starting with this low-entropy state, the sample is compressed using a small initial shock (< 0.2 GPa) followed by a pressure ramp that approaches isentropic loading as the sample is taken to hundreds of GPa. Planar loading allows for quantitative compression measurements, the objective of our low-entropy compression being to keep the sample cold enough to characterize crystalline hydrogen toward the terapascal (TPa) range.

I. Introduction

The metallization of hydrogen under high pressures was first conceived by Wigner and Huntington¹ in 1935. Later work additionally predicted that high-density hydrogen could exhibit high temperature superconductivity²⁻³, become a superconducting superfluid⁴, and form superconducting metal hydrides⁵, raising significant interest in the quantum nature of dense hydrogen. Recent DFT-based studies suggest that at pressures above 500 GPa, the solid transitions to an atomic superconductor⁶⁻⁸. Experimentally, diamond anvil cell studies discovered a rich polymorphism of the molecular solid between 100 – 400 GPa using Raman⁹⁻¹¹, infrared¹²⁻¹³, electrical¹⁴, and X-ray¹⁵ diagnostics. Recently, these experiments reached pressures between 425 – 440 GPa in the solid, observing an insulator to conductor transition at pressures around 350 – 360 GPa¹⁶⁻¹⁷.

Shock compression of pre-compressed¹⁸ or cryogenic¹⁹⁻²⁰ liquid hydrogen revealed a transition from electrically insulating to conducting fluid around 12 kK and 50 GPa. Ramp compression of cryogenic deuterium²¹⁻²² successfully accessed lower temperatures of a couple thousand K and a few hundred GPa, also observing the fluid-fluid insulator-conductor transition (see figure 1). These dynamic compression experiments are able to reach pressures exceeding 700 GPa, but require careful design to limit the temperature increase. The present work discusses the use of minimum entropy targets, as well as custom laser pulse-shaping, to achieve near-isentropic compression to hundreds of GPa, and toward the quantum regime where the thermal wavelength exceeds the interatomic spacing (see figure 1).

An approach to limit the entropy of the target before and during compression is outlined in the next section. Details on the target fabrication are presented in the final section.

18 June 2025 14:18:07

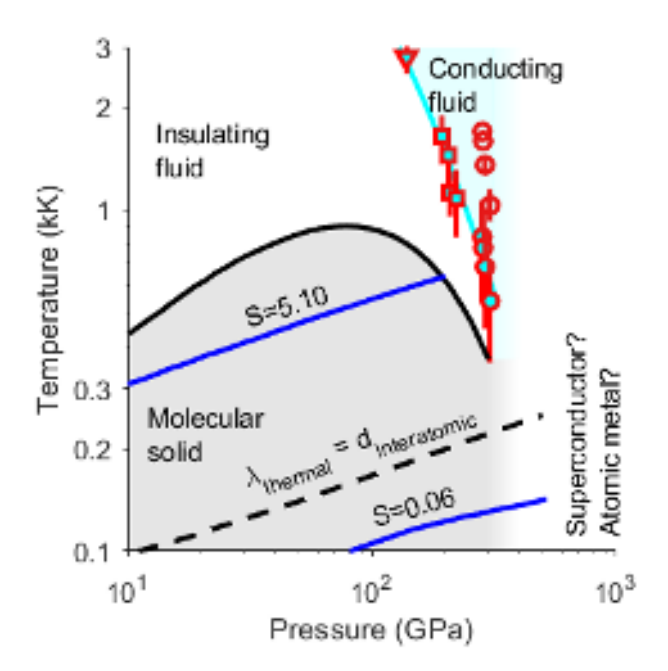


FIG. 1. Schematic pressure-temperature hydrogen phase diagram including the particular region of interest around 500 GPa and 500 K. The aim is to extend the dynamic studies compressing liquid deuterium and hydrogen into the electrically conducting regime (triangle²³, squares²¹ and dots²²) to lower temperatures. Two isentropes are shown for liquid normal deuterium (entropy S = 5.1 $k_{B}/molecule$: Boltzmann constant k_{B}), and solid j = even hydrogen targets (S = 0.06 $k_{B}/molecule$), indicating that isentropically compressed crystalline para (j = even) hydrogen targets can reach

²Laboratory for Laser Energetics, 250 East River Rd, 14623, Rochester, New York, USA

³Department of Chemistry, University of Rochester, Rochester, New York, 14611, USA

⁴Department of Earth and Planetary Science, University of California Berkeley, Berkeley, California, 94720, USA

⁵Lawrence Livermore National Laboratory, 7000 East Avenue, 94550, Livermore, California, USA

^{*}Author to whom correspondence should be addressed: aschwemm@ur.rochester.edu

PLEASE CITE THIS ARTICLE AS DOI: 10.1063/5.0205013

6/2/2024 RSI24-AR-00370

the atomic state. The melt curve was taken from Ref 9, the interatomic spacing from ref 15.

II. Feasibility of dynamic compression experiments with minimum entropy targets

One strategy for achieving lower temperatures in dynamic compression experiments is to isentropically compress low initial-entropy samples. Such compression paths are adiabatic because the hydrodynamic timescales are significantly shorter than heat conduction timescales. It is plausible to achieve low-temperature states in dynamic experiments through non-adiabatic processes, but these will not be discussed here. This paper describes how to achieve a low initial entropy for hydrogen, and a pulse-shaping strategy for enabling near isentropic compression at the OMEGA 60 laser facility.

The hydrogen molecule consisting of two spin ½ protons can be in the ortho state (total spin j = odd) or in the para state (total spin j = even). Normal hydrogen consists of 75% j = odd and 25% j = even hydrogen in equilibrium at room temperature²⁴. On the other hand, the deuterium molecule consists of two spin 1 nuclei, which at room temperature form a population of 67% j = even and 33% j = odd. At cryogenic temperatures, j = even hydrogen has lower entropy than normal (let alone ortho) hydrogen. Lower temperatures also reduce the entropy, and there is a significant reduction in entropy upon solidification. Figure 2 shows the entropy of pure j=even hydrogen compared to normal hydrogen and deuterium as a function of temperature, in the vicinity of the melting transitions. The entropies for the solid were calculated using the Driessen-Silvera equation of state (EOS)²⁵, whereas the entropies for the liquid use Saumon's EOS²⁶.

Previous studies used deuterium targets since they achieve higher pressures with a given driver in shock experiments²¹⁻²³. Additionally, deuterium is a closer isotopic surrogate to fusion fuel consisting of deuterium and tritium. For this study, hydrogen targets are preferred because the different nuclear spin statistics of hydrogen enable much lower initial entropies (compare figures 2, 3 and 4). In addition, the thermal wavelength at a given temperature (compare figure 1) is longer for hydrogen than for deuterium, making quantum effects accessible at higher temperatures.

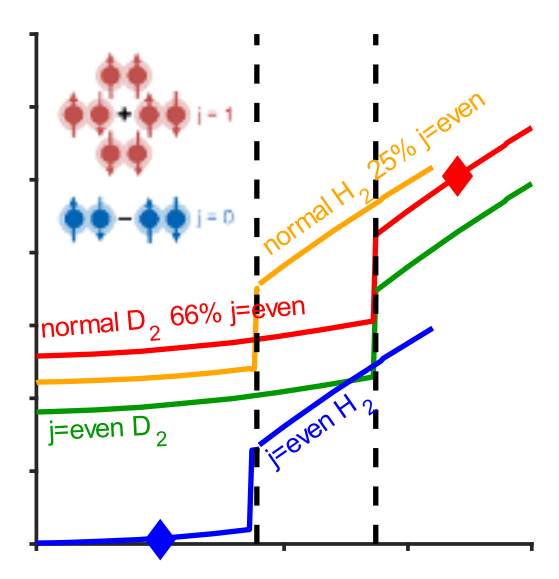


FIG. 2. Entropy of j = even hydrogen, deuterium, normal hydrogen and normal deuterium as a function of temperature at 1 bar. OMEGA targets can be cooled down to 10 K, resulting in a 0.06 $k_{\text{B}}/\text{molecule}$ j = even hydrogen target. Isentropes for 10 K j = even hydrogen and 21.5 K normal deuterium (diamonds) are shown in figure 1. Previous experiments 21 used liquid normal deuterium at 21.5 K, thus with 5.1 $k_{\text{B}}/\text{molecule}$, whereas the present study uses solid j = even hydrogen at 10 K and 0.06 $k_{\text{B}}/\text{molecule}$.

Currently, ~10 K initial temperature is achievable within a shot cycle using the OMEGA planar cryogenic platform, which is low enough for hydrogen to be in the crystalline phase with less than 0.1 k_B/molecule of entropy for a i =even sample (k_B: Boltzmann constant). Isentropes calculated with Chabrier's hydrogen EOS²⁷, using the entropies from Fig. 2, are shown in Fig 1 for liquid normal deuterium targets at 21.5 K and solid j = even hydrogen targets at 10 K. These results suggest that isentropic compression of solid i = 1even hydrogen can access the atomic metallic state. At ~500 GPa, the calculated temperature is 140 K. This simple estimate also suggests that an isentrope < 1.2 k_B/molecule can reach the crystalline monatomic state of hydrogen. However, this calculation assumes an equilibrium ratio of j =even hydrogen at every temperature. Therefore, it does not take into account the latent heat associated with changes in rotational states that might occur during compression. Furthermore, the latent heat of other phase transitions in the solid was also neglected, which may produce significant jumps in the temperature. The given temperature is therefore likely an overestimate.

To take full advantage of the initial low entropy of solid j= even hydrogen targets, a near-isentropic drive is needed. A recent study²¹ at the National Ignition Facility (NIF) employed a drive consisting of an initial shock and a 20 ns ramp. The liquid normal deuterium targets (21.5 K, S = 5.1 k_B /molecule) were shocked to 2.5 GPa and an entropy of 13.1 k_B /molecule (Fig. 3). From this point, the ramp

PLEASE CITE THIS ARTICLE AS DOI: 10.1063/5.0205013

6/2/2024 RSI24-AR-00370

compression increased the pressure to a final 390 GPa. The spin state was not accounted for in the analysis of the experiment in temperature – pressure space. However, the entropy difference between normal deuterium and equilibrated deuterium at 21.5 K was added to the analysis in entropy – pressure space. Here, entropy is interpreted as the number of accessible microstates at a given temperature. This experiment observed the liquid insulating to conducting transition in hydrogen (Fig. 4).

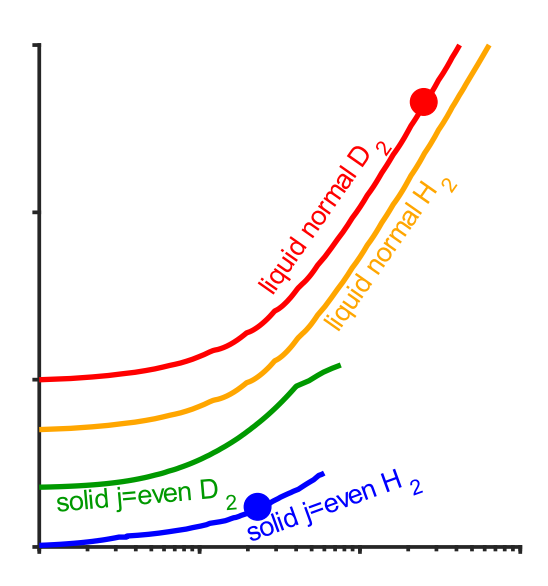


FIG. 3: Entropy increase as function of first shock pressure, using Ref 25 for the solid and Ref 26 for the liquid. To access the 1.2 $k_{\text{B}}/\text{molecule}$ isentrope reaching the solid atomic state, the first shock in crystalline j=even hydrogen should not exceed 0.2 GPa (blue dot). A previous NIF study²¹ produced a shock of 2.5 GPa in liquid deuterium, giving an entropy of 13.1 $k_{\text{B}}/\text{molecule}$ (red dot). Note that the solid deuterium starts to follow the melt curve above 0.34 GPa, whereas hydrogen encounters it at 0.03 GPa due to the lower melting temperature. Shocked solid hydrogen would fully melt at 0.55 GPa, whereas deuterium would melt at 0.74 GPa. The described initial shock remains well below this limit.

Similar drives were designed and tested at the OMEGA 60 laser facility. OMEGA 60 consists of 60 individual laser beams that converge uniformly on a spherical target, of which 12 beams can be efficiently coupled to a planar target. Frequency conversion shifts the infrared radiation from the Nd:glass laser to 351 nm. Each beam can deliver up to 500 J during a pulse length of up to .37 ns, with a minimum spot size diameter of 0.4 mm. The temporal evolution of the intensity during this pulse can be selected by the user, and multiple pulses can be temporally stitched together. This spherical drive geometry, designed for inertial fusion experiments²⁸, limits the available energy and maximum compression time for planar targets. Therefore, a weak

initial shock is used that increases the sound speed in the hydrogen from 1.5 km/s to 3.1 km/s, which reduces the duration of the following ramp to 16 ns. This shock was limited to 0.2 GPa, generating a calculated increase in entropy of 1.2 k_B/molecule (Fig. 3). Similar to the NIF experiment, a final ramp then compresses the target nearly isentropic to more than 500 GPa (Fig. 4: *blue curves*). A conceivable experiment using the same drive on solid j=even deuterium at 10 K crosses the melt line at 570 K (*green curves* in figure 4).

Although there is considerable experience compressing crystalline deuterium in spherical geometries²⁸, the present study focuses on planar compression experiments because these provide the most controlled and therefore quantitative characterization of the sample under dynamic loading¹⁹⁻²³. Indeed, we are aware of only one previous study²⁹ of crystalline hydrogen in planar dynamic compression, to a maximum pressure of 0.7 GPa.

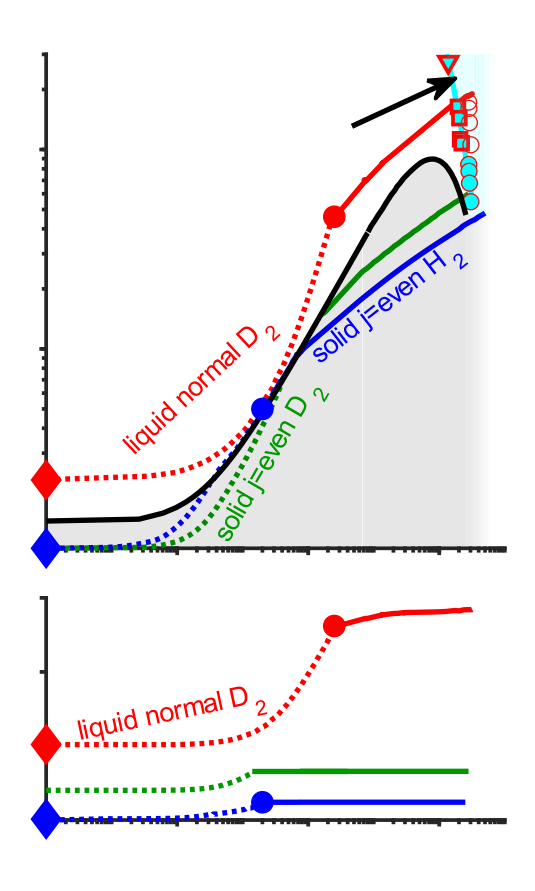


FIG. 4. Phase diagram of hydrogen including dynamic compression paths using liquid normal deuterium (red curves), solid j=even hydrogen (blue curves) and solid j=even deuterium targets (green curves); initial states for solid j=even hydrogen and liquid normal deuterium are indicated by diamonds. Near-isentropic compression (solid curves) is achieved after the first shock (dashed curves) to 1.2 k_B/molecule for solid j=even hydrogen and 13.1 k_B/molecule for liquid normal deuterium. Solid j=even hydrogen targets can reach the solid

PLEASE CITE THIS ARTICLE AS DOI: 10.1063/5.0205013

6/2/2024 RSI24-AR-00370

atomic state of hydrogen. Three prior studies (cyan triangle²³, squares²¹ and dots²²) compressed liquid deuterium into the liquid conducting regime. The melt curve was taken from references 9 and 30 and assumes an equilibrium ratio of spin states at every temperature.

III. Solid j = even hydrogen target preparation at the OMEGA facility

High purity j= even hydrogen can be produced by cooling normal hydrogen gas to low temperatures (< 20 K) and waiting for self-conversion of j= odd to j= even molecules to its thermal equilibrium of < 0.2%. However, this process takes hundreds of hours, and thus is not suitable for target production. In the present work, hydrogen gas was brought into contact with a paramagnetic catalyst at 20 K, which produces the equilibrium j= even concentration within seconds. This procedure is realized on an industrial scale and is well documented³¹.

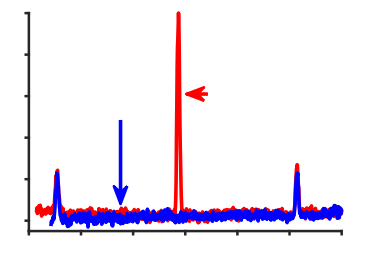
For target production, a miniaturized j = even hydrogen generator was developed in an on-site laboratory from where targets can be transferred to the OMEGA target chamber within minutes. The generator consists of a commercial cryostat (ColdEdge Stinger) capable of cooling the converter to a minimum temperature of 14 K. The converter consists of a 1/8" diameter refrigerator-grade copper spiral, filled with iron (III) oxide (hydrated, catalyst grade, 30-50 mesh). The ends of the spiral are equipped with particle filters to confine the powder. As ultra-high purity (99.999%) hydrogen flows through this spiral, it cools down and is converted to the j = even state. After conversion, the j = evenhydrogen is brought back up to room temperature and contained in Cu-lined vessels that limit the i = even to i = even toodd conversion. The vessels were custom-made by electroplating copper onto a standard stainless steel micro-ConFlat tee. The two opposite ends of the tee were equipped with standard sapphire windows to enable Raman spectroscopy, while the remaining end was attached to a vacuum valve.

The purity of the j = even hydrogen produced in the converter as well as the back conversion rate at room temperature were documented by Raman spectroscopy³² (Fig. 5). The Raman diagnostic setup is similar to that in Ref. 33, and operates with a 100 mW diode-pumped solidstate laser at 532 nm (LRS-0532, Laserglow Technologies). A broadband non-polarizing beam splitter (120BC17MB.1, Newport) directs the laser light to a lens (AC254-075-A-ML, Thorlabs) which focuses the probe into 2 atm of room temperature j = even hydrogen stored in the vessel describedabove. The Raman-scattered radiation is collected in backscattering geometry by the same lens and passed back through the beam splitter to another lens (AC254-150-A-ML, Thorlabs) that focuses the Raman-scattered light onto the spectrometer (SpectraPro HRS-500, Princeton Instruments) through a series of 3 OD6 notch filters (#86130, Edmund Optics) that remove the residual 532 nm light from the laser.

The j=0 to j=2 transition (354 cm⁻¹) and the j=1 to j=3 transition (568 cm⁻¹) from the resulting spectra were used to quantify the j= odd concentration in the sample, taking into account the ratio of Boltzmann factors²⁴ and Raman cross sections³⁴ for both levels. Due to the Pauli principle, j= even hydrogen can only occupy even rotational states, and j= odd only odd ones.

Normal hydrogen produces a dominant peak at the expected 586 cm⁻¹, corresponding to a j = odd concentration of 75% (figure 5). The j = even hydrogen product, on the other hand, produces no recognizable transition in this region. The statistical uncertainty of the j = odd concentration found at higher j = odd concentrations is approximately 3%, which is above the expected 0.2% equilibrium concentration of the hydrogen product.

The conversion rate at room temperature of this j= even hydrogen sample back to the room temperature equilibrium ratio was measured using the same method to be 0.11 ± 0.01 %/h (\pm statistical error). For this measurement, the j= even hydrogen was kept in the described vessel, and the j= odd concentration was periodically measured (see figure 5). It was assumed that the product started at 0.2% j= odd concentration, the expected equilibrium ratio during production, and that the increase follows a linear trend with time at low j= odd concentrations. The targets are typically shot within 2 h of generation, giving an acceptable j= odd concentration under 0.4 ± 0.02 %.



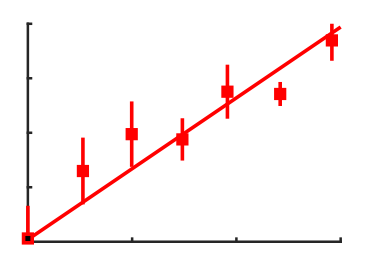


FIG. 5. Top: Representative Raman spectrum, with background removed, of normal hydrogen from the bottle and j = even hydrogen

PLEASE CITE THIS ARTICLE AS DOI: 10.1063/5.0205013

6/2/2024

from the generator immediately after generation. The peak at 586 cm⁻¹ is caused by the j=1 to j=3 transition (j= odd), the peaks at 354 cm⁻¹ and 815 cm⁻¹ correspond to the j=0 to j=2 and j=2 to j=4 transitions (j= even hydrogen). In the sample from the generator, no ortho-hydrogen could be detected within the statistical uncertainty for a single measurement of 3%. Bottom: j= odd fraction of a sample as a function of time, approaching the equilibrium ratio of 75%. Based on this time series, the residual j= odd hydrogen in the product is $\leq 0.4\% \pm 0.02\%$.

For dynamic compression experiments, the gaseous j=even hydrogen is filled into a 10 cc reservoir attached to the planar target. To limit the j= odd conversion, the reservoir was machined from refrigerator-grade copper tubing. As the target is cooled, hydrogen flows from the reservoir and condenses in the target (see figure 6), ultimately to form a 20 μ m thick layer of solid j=even hydrogen. The quality of the hydrogen layer is monitored in real time by imaging through the lithium fluoride window and the transparent hydrogen reservoir using the existing velocity interferometer (VISAR³⁵) imaging system. (Fig. 7)

To grow a high-quality, uniform (hcp) crystal³⁶⁻³⁷ of hydrogen, careful temperature control is required for the target. This is a well-documented process in inertial confinement fusion experiments, where the decay of tritium provides a volumetric heat source that preferably melts thicker areas³⁷. A similar heat source can also be established by infrared pumping certain molecular levels³⁸⁻³⁹. Here, a temperature gradient of about 0.1 K was established across the hydrogen, to encourage uniform crystal growth toward the camera (Fig. 6). In addition, the temperature follows a custom profile that was optimized for this particular application. In a first step, the hydrogen is brought below the freezing temperature (13.7 K for i = even hydrogen) at a rate of 0.5 K/min. This initial crystallization typically causes voids that are removed by slowly approaching the melting temperature again (Fig. 7). The solid now partially melts, so channels can form between the voids and the fill tube, which allow additional hydrogen to flow in and fill the voids.

Clear visual indications of liquefaction and solidification are observed and used to determine the state of the hydrogen sample and to calibrate our thermometry.

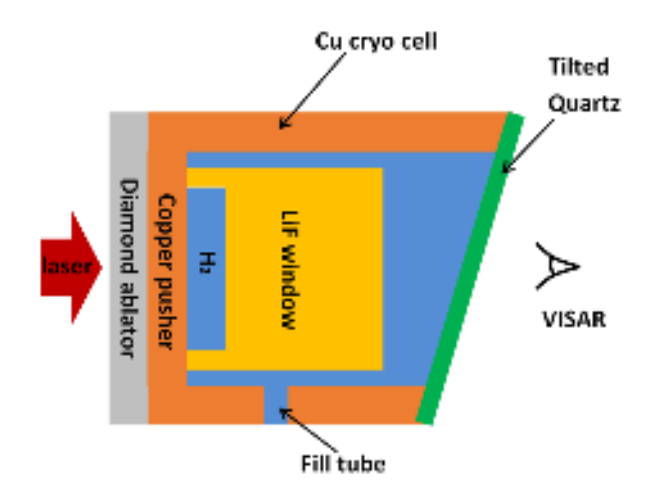
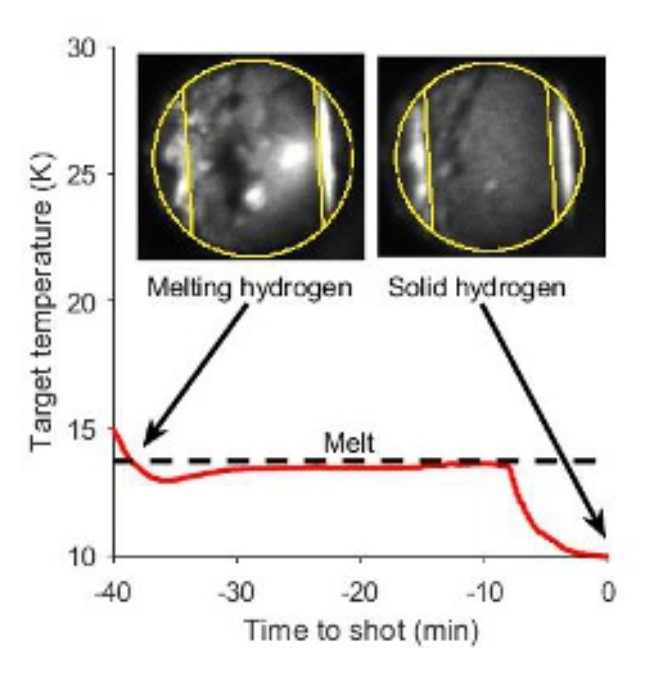


FIG. 6. Side view of the target. The VISAR camera looks through the lithium fluoride (LiF, 250 μm thickness) and hydrogen (20 μm thick) onto the copper (20 μm thick). The LiF encloses only the sides of the H_2 target (compare figure 7), so that the hydrogen can flow from the fill tube into the target.

Homogeneous targets of j = even crystalline hydrogen were produced using this method within the 90 minute shot cycle of the OMEGA facility (Fig. 7). After the imperfections in the solid hydrogen were removed, the targets were cooled within 8 minutes to the experimental temperature of 10 K, and then continuously kept cooled until six seconds before the shot. At six seconds before laser-produced compression, the cryogenics are turned off to prevent target motion from the mechanical refrigerator. During this time, the sample stays at the operating temperature due to the large thermal mass (23 g) of the copper cryogenic cell confining the hydrogen (for comparison, the mass of the H_2 sample is less than one mg).



PLEASE CITE THIS ARTICLE AS DOI: 10.1063/5.0205013

6/2/2024 RSI24-AR-00370

FIG. 7. Temperature history designed for solid hydrogen formation (red curve). The initial cooling below the melt temperature causes voids, which are subsequently removed by approaching the melt temperature again. In some cases, multiple crossings of the melt are necessary to improve the quality of the ice layer that has a final temperature of 10 K. The two snapshots show the target during a phase transition from liquid to solid, and the final solid hydrogen. Note the homogeneous solid layer. The bright structures on the left and right are the edges of the LiF window, as indicated by the yellow mask. The dark triangle on the top left in the solid hydrogen is glue on the window.

IV. Summary

Probing crystalline hydrogen at low temperatures and terapascal pressures as well as searching for characterizing its predicted novel physics superconductivity²⁻³, atomic solids⁶⁻⁸, and more remains one of the grand challenges of physics. To enable dynamic compression experiments exceeding 500 GPa in the solid state, a new platform is under development at OMEGA. While previous dynamic compression experiments have reached these pressures, temperatures of a few thousand K were generated. To access the solid at high pressures, minimum entropy ($< 0.1 \text{ k}_B/\text{molecule}$) j = even crystalline hydrogen targets are driven near-isentropically. The j = evenhydrogen is produced and diagnosed using Raman spectroscopy in an on-site lab. High-quality j = even hydrogen crystals were grown in-situ in the OMEGA target chamber by establishing a small temperature gradient in the target and following an optimized temperature profile. The near-isentropic compression path of this target consists of a weak shock pre-compression to approximately 0.2 GPa, followed by ramp compression to > 500 GPa at temperatures calculated to remain below 500 K.

Acknowledgements

The authors thank Didier Saumon for valuable discussions regarding his equation of state table for hydrogen. Furthermore, the authors thank the Laboratory for Laser Energetics' cryogenic facility personnel Roger Janezic, Sean Adams, Chad Fella and Robert Earley for their assistance in growing uniform solid hydrogen crystals.

This material is based upon work of the Center for Matter at Atomic Pressures (CMAP), supported by the National Science Foundation under Grant No. PHY-2020249. Any opinions, findings, and conclusions or recommendations expressed in this material are those of the author(s) and do not necessarily reflect the views of the National Science Foundation.

This material is based upon work supported by the Department of Energy National Nuclear Security Administration under Award Number DE-NA0003856, the University of Rochester, and the New York State Energy

This material is based upon work supported by the U.S. Department of Energy, Office of Science, Office of Fusion Energy Sciences, Quantum Information Science program under Award Number DE-SC-0020340.

This work was performed under the auspices of the U.S. Department of Energy by Lawrence Livermore National Laboratory under Contract DE-AC52-07NA27344.

The data that support the findings of this study are available from the corresponding author upon reasonable request.

References

- ¹E. Wigner and H. B. Huntington, J. Chem. Phys. **3**, 764 (1935).
- ²J. E. Jaffe and N. W. Ashcroft, Phys. Rev. B **23**, R6176 (1981).
- ³N. W. Ashcroft, Phys. Rev. Lett. **21**, 1748 (1968).
- ⁴E. Babaev, A. Sudbo, and N. W. Ashcroft, Nature **431**, 666 (2004).
- ⁵N. W. Ashcroft, Phys. Rev. Lett. **92**, 187002 (2004).
- ⁶J. M. McMahon and D. M. Ceperley, Phys. Rev. B **84**, 144515 (2011).
- ⁷J. McMinis, R. C. Clay, D. Lee, and M. A. Morales, Phys. Rev. Lett. **114**, 105305 (2015).
- ⁸L. Monacelli, M. Casula, K. Nakano, S. Sorella, and F. Mauri, Nat. Phys. **19**, 845 (2023).
- ⁹R. T. Howie, P. Dalladay-Simpson, and E. Gregoryanz, Nat. Mater. **14**, 495 (2015).
- ¹⁰P. Dalladay-Simpson, R. T. Howie, and E. Gregoryanz, Nature **529**, 63 (2016).
- ¹¹C. Zha, H. Liu, J. S. Tse, J. Hemley, Phys. Rev. Letters **119**, 075302 (2017)
- ¹²C. Zha, Z. Liu, and R. J. Hemley, Phys. Rev. Letters **108**, 146402 (2012)
- ¹³B. Edwards and N. W. Ashcroft, PNAS **101** (**12**), 4013-4018 (2004)
- ¹⁴M. I. Eremets and I. A. Troyan, Nat. Mater. **10**, 927 (2011).

accepted manuscript. However, the online version of record will be different from this version once it has been copyedited and typeset

PLEASE CITE THIS ARTICLE AS DOI: 10.1063/5.0205013

This is the author's peer reviewed,

¹⁵C. Ji, B. Li, W. Liu, J. S. Smith, A. Majumdar, W. Luo, R. Ahuia, J. Shu, J. Wang, S. Sinogeikin, Y. Meng, V. B.

Ahuja, J. Shu, J. Wang, S. Sinogeikin, Y. Meng, V. B. Prakapenka, E. Greenberg, R. Xu, X. Huang, W. Yang, G. Shen, W. L. Mao, and H.-K. Mao, Nature **573**, 558 (2019).

¹⁶P. Loubeyre, F. Occelli, and P. Dumas, Nature **577**, 631 (2020).

¹⁷M. I. Eremets, A. P. Drozdov, P. P. Kong, and H. Wang, Nat. Phys. **15**, 1246 (2019).

¹⁸P. Loubeyre, S. Brygoo, J. Eggert, P. M. Celliers, D. K. Spaulding, J. R. Rygg, T. R. Boehly, G. W. Collins, and R. Jeanloz, Phys. Rev. B **86**, 144115 (2012).

¹⁹G. W. Collins, L. B. Da Silva, P. Celliers, D. M. Gold, M. E. Foord, R. J. Wallace, A. Ng, S. V. Weber, K. S. Budil, and R. Cauble, Science **281**, 1178 (1998).

²⁰P. M. Celliers, G. W. Collins, L. B. Da Silva, D. M. Gold, R. Cauble, R. J. Wallace, M. E. Foord, and B. A. Hammel, Phys. Rev. Lett. **84**, 5564 (2000).

²¹P. M. Celliers, M. Millot, S. Brygoo, R. S. McWilliams, D. E. Fratanduono, J. R. Rygg, A. F. Goncharov, P. Loubeyre, J. H. Eggert, J. L. Peterson, N. B. Meezan, S. Le Pape, G. W. Collins, R. Jeanloz, and R. J. Hemley, Science **361**, 677 (2018).

²²M. D. Knudson, M. P. Desjarlais, A. Becker, R. W. Lemke, K. R. Cochrane, M. E. Savage, D. E. Bliss, T. R. Mattsson, and R. Redmer, Science **348**, 1455 (2015).

²³S. T. Weir, A. C. Mitchell, and W. J. Nellis, Phys. Rev. Lett. **76**, 1860 (1996).

²⁴P. C. Souers, in *Hydrogen Properties for Fusion Energy* (University of California, Berkeley, CA, 1986), p. 26.

²⁵A. Driessen and Isaac F. Silvera, J. Low Temp. Phys. **54**, 565 (1984).

²⁶D. Saumon, *The SESAME 5267 Equation of State of Deuterium*, Los Alamos National Laboratory, Los Alamos, NM, Report LA-UR-08-0303 (2007).

²⁷G. Chabrier, S. Mazevet, and F. Soubiran, Astrophys. J. **872**, 51 (2019).

²⁸V. Gopalaswamy, R. Betti, J. P. Knauer, N. Luciani, D. Patel, K. M. Woo, A. Bose, I. V. Igumenshchev, E. M.

RSI24-AR-00370

Campbell, K. S. Anderson, K. A. Bauer, M. J. Bonino, D. Cao, A. R. Christopherson, G. W. Collins, T. J. B. Collins, J. R. Davies, J. A. Delettrez, D. H. Edgell, R. Epstein, C. J. Forrest, D. H. Froula, V. Yu. Glebov, V. N. Goncharov, D. R. Harding, S. X. Hu, D. W. Jacobs-Perkins, R. T. Janezic, J. H. Kelly, O. M. Mannion, F. J. Marshall, D. T. Michel, S. Miller, S. F. B. Morse, J. P. Palastro, J. Peebles, P. B. Radha, S. P. Regan, S. Sampat, T. C. Sangster, A. B. Sefkow, W. Seka, R. C. Shah, W. T. Shmayda, A. Shvydky, C. Stoeckl, A. A. Solodov, W. Theobald, J. D. Zuegel, M. Gatu Johnson, R. D. Petrasso, C. K. Li, and J. A. Frenje, Nature 565, 581 (2019).

²⁹P. L. Lagus and T. J. Ahrens, J. Chem. Phys. **59**, 3517 (2003).

³⁰D. H. Liebenberg, R. L. Mills, and J. C. Bronson, Phys. Rev. B **18**, 4526 (1978).

³¹B. Feng, A. M. Coffey, R. D. Colon, E. Y. Chekmenev, and K. W. Waddell, J. Magn. Reson. **214**, 258 (2012).

³²L.-M. Sutherland, J. N. Knudson, M. Mocko, and R. M. Renneke, Nucl. Instrum. Methods Phys. Res. A. **810**, 182 (2016).

³³C. Rathmell and D. Chen, Spectroscopy Supplements **33** (2018).

³⁴A. L. Ford and J. C. Browne, At. Data Nucl. Data Tables **5**, 305 (1973).

³⁵P. M. Celliers, D. K. Bradley, G. W. Collins, D. G. Hicks, T. R. Boehly, and W. J. Armstrong, Rev. Sci. Instrum. **75**, 4916 (2004).

³⁶G. W. Collins, P. C. Souers, F. Magnotta, E. R. Mapoles, and J. R. Gaines, Phys. Rev. B **53**, 8143 (1996).

³⁷B. J. Kozioziemski, G. W. Collins, and T. P. Bernat, Fusion Technology **31**, 482 (1997).

³⁸D. N. Bittner, G. W. Collins, E. Monsler, and S. Letts, Fusion Technol. **35**, 244 (1999).

³⁹G. W. Collins, D. N. Bittner, E. Monsler, S. Letts, E. R. Mapoles, and T. P. Bernat, J. Vac. Sci. Technol. A **14**, 2897 (1996).